

Mediation of Ultrafast Light-Harvesting by a Central Dimer in Phycoerythrin 545 Studied by Transient Absorption and Global Analysis

Alexander B. Doust,[†] Ivo H. M. van Stokkum,[‡] Delmar S. Larsen,^{‡,||} Krystyna E. Wilk,[§] Paul M. G. Curmi,[§] Rienk van Grondelle,^{*,‡} and Gregory D. Scholes^{*,†}

Lash Miller Chemical Laboratories, 80 St. George Street, University of Toronto, Ontario, M5S 3H6 Canada, Department of Physics and Astronomy, Faculty of Sciences, Vrije Universiteit, De Boelelaan 1081, 1081 HV Amsterdam, The Netherlands, and School of Physics, The University of New South Wales, Sydney, N.S.W. 2052, Australia

Received: March 7, 2005; In Final Form: May 30, 2005

We report ultrafast femtosecond transient absorption measurements of energy-transfer dynamics for the antenna protein phycoerythrin 545, PE545, isolated from a unicellular cryptophyte *Rhodomonas CS24*. The phycoerythrobilins are excited at both 485 and 530 nm, and the spectral response is probed between 400 and 700 nm. Room-temperature measurements are contrasted with measurements at 77 K. An evolution-associated difference spectra (EADS) analysis is combined with estimations of bilin spectral positions and energy-transfer rates to obtain a detailed kinetic model for PE545. It is found that sub pulse-width dynamics include relaxation between the exciton states of a chromophore dimer ($\beta 50/60$) located in the core of the protein. Energy transfer from the lowest exciton state of the phycoerythrobilin (PEB) dimer to one of the periphery 15,16-dihydrobiliverdin (DBV) bilins is found to occur on a time scale of 250 fs at room temperature and 960 fs at 77 K. A host of energy-transfer dynamics involving the $\beta 158$, $\beta 82$, and $\alpha 19$ bilins occur on a time scale of 2 ps at room temperature and 3 ps at 77 K. A final energy transfer occurs between the red-most DBV bilins with a time scale estimated to be ~ 30 ps. The role of the centrally located phycoerythrobilin dimer is seen as crucial—spectrally as it expands the cross-section of absorption of the protein; structurally as it sits in the middle of the protein acting as an intermediary trap; and kinetically, as the internal conversion and subsequent red-shift of the excitation is extremely fast.

Introduction

In photosynthesis, light-harvesting antenna proteins bind chromophores belonging to one of three classes: chlorophylls, carotenoids, and phycobilins. In cyanobacteria and red algae, the major light-harvesting antenna complexes are phycobiliproteins (PBPs) that contain phycobilins—linear tetrapyrrole chromophores that absorb predominantly green light, but also absorb in the red spectral region. The PBPs are organized into large, multiprotein phycobilisome (PBS) complexes that are bound to the stromal face of the thylakoid membrane, and they have been studied in great detail.^{1–9} Cryptophyte algae also contain antenna proteins with phycobilin chromophores; however, the mechanism of light-harvesting is significantly different from that of the phycobilisomes of the cyanobacteria and red algae.^{1,2,10–13} It is therefore of interest to elucidate the operation of the bilin-containing peripheral light-harvesting complex phycoerythrin 545 (PE545) in a cryptophyte algae.

The ultrahigh-resolution crystal structure model reveals that PE545 contains eight bilins, separated by typical distances of 20–45 Å¹⁰ (Figure 1). An interesting aspect of the structure is

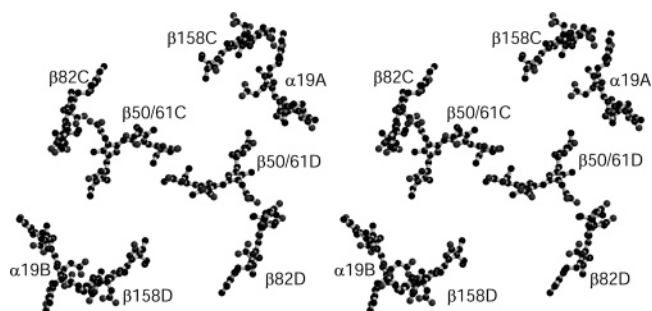


Figure 1. Stereoview of the organization of the pigments in PE545. The stacking orientation of the terminal pyrrole units of the central $\beta 50/\beta 61$ pair in the middle of the figure is clear to see. One of the two $\alpha 19$ bilins is responsible for emission.

that it contains a dimer composed of two phycoerythrobilin molecules whose terminal conjugated pyrrole rings sit on top of each other in such a way that the closest atom-to-atom distance is only 2 Å. This structural motif is much like the special pair of bacteriochlorophyll-*a* molecules in the reaction center of purple bacteria¹⁴ or allophycocyanin in PBS.^{15,16} Chromophore dimers are common in photosynthetic proteins. Importantly, their spectroscopic properties are modified from the monomeric constituents,¹⁷ allowing for mixing of states and significantly altered absorption features. For example, the optical properties and light-harvesting dynamics of the FMO complex^{18,19} and LH2^{20–22} are very closely tied to the strong excitonic interactions between neighboring pigments. Thus we are motivated to determine the role of the dimer in PE545 for

* Corresponding authors. (van Grondelle) Phone: (+31) 20 5987930. Fax: (+31) 20 5987999. E-mail: R.van.Grondelle@few.vu.nl. (Scholes) Phone: (+1) 416 9467532. Fax: (+1) 416 9788775. E-mail: gscholes@chem.utoronto.ca.

[†] University of Toronto.

[‡] Vrije Universiteit.

[§] University of New South Wales.

^{||} Present address: Department of Chemistry, University of California, 1 Shields Ave., Davis, CA 95616.

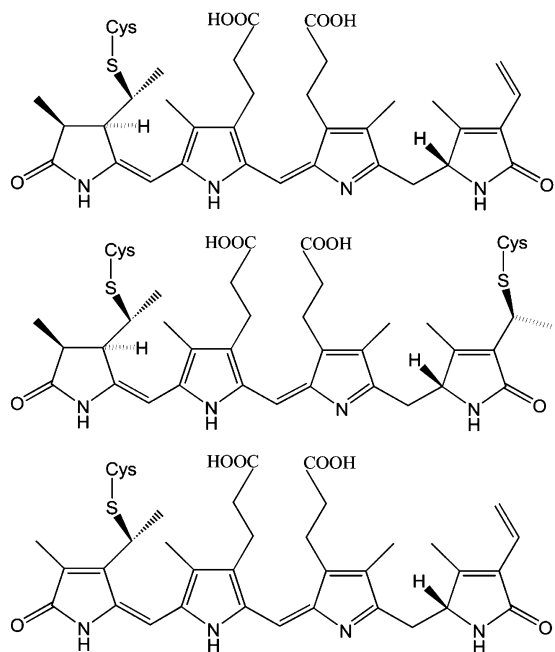


Figure 2. The chemical structures of the bilins. Top, the standard PEB chromophore as per $\beta 82$ and $\beta 158$; middle, the doubly linked $\beta 50/60$; and bottom, the $\alpha 19$ chromophore.

light-harvesting and energy transfer. To that effect, we report here femtosecond transient absorption measurements that expose the ultrafast energy-transfer and trapping dynamics in PE545.

In cryptophytes, there are no large bilisome structures. Only one type of PBP is present in a single species, either phycocyanin or phycoerythrin and never allophycocyanin. The protein is located in the thylakoid lumen, which is unique to the cryptophytes and dinoflagellates.²³ The structure of PE545, isolated from the unicellular cryptophyte *Rhodomonas CS24*, has been determined at 0.97-Å resolution,¹⁰ clearly showing the positions, orientations, local protein environment, and even conformational differences of the eight bilins (Figure 1). PE545 has dimensions which are $75 \times 60 \times 45$ Å and is a $(\alpha_1\beta)(\alpha_2\beta)$ heterodimeric protein rather than a trimer as in the PBS. Each $\alpha\beta$ monomer unit contains three phycoerythrobilins (PEB) and one dihydrobiliverdin (DBV) pigments on the β - and α -subunits, respectively (Figure 2). The three β -subunit chromophores, $\beta 50/\beta 61$, $\beta 82$, and $\beta 158$, are all phycoerythrobilins (PEBs) with conserved bilin location on the polypeptide chain. The $\beta 82$ and $\beta 158$ chromophores are covalently linked to the apoprotein by a single cysteine bond, while the $\beta 50/\beta 61$ chromophore is doubly linked. The α -subunit chromophore is a singly linked 15,16-dihydrobiliverdin (DBV), which has increased conjugation in the pyrrole A ring compared to the PEBs,¹ and it is thus red-shifted compared to the PEB bilins.

Although the β -subunits of the cryptophytes share a high degree of sequence identity with both the α - and β -subunits of cyanobacteria and red algae, their α -subunits are shorter, unrelated to other proteins in the sequence databases, and carry a single, spectroscopically distinct bilin chromophore.²⁴ Cryptophytes contain, besides phycobiliproteins, chlorophyll-*c2*; this combination is unique and may allow greater photosynthetic activity. One of the DBV bilins in PE545 is the final acceptor of the excitation and is responsible for emission in vitro and energy transfer to chlorophyll in vivo. PE545 has a strong absorbance at 545 nm and a major fluorescence emission at 585 nm.^{10,25–28} The primary function of this remarkable light-harvesting apparatus is to allow the organism to survive in weak light conditions. As green light is transmitted through greater

depths of water where the organism resides, PE545 possesses the particular ability to absorb photons in the spectral regions where light is only weakly absorbed by chlorophylls and carotenoids and to funnel this absorbed energy preferentially to PS-II.^{29–31}

The tuning of the spectroscopic properties of the bilins is crucial in adapting these chromophores to their functions in photosynthesis.^{29,32} It involves complex noncovalent interactions, mainly with the apoprotein, but also with neighboring chromophores,^{11,29,33–35} allowing only two bilin types to cover 100 nm or 3500 cm^{-1} of the visible spectrum between the Soret and Q_y bands of chlorophyll-*a*. Free phycobilins have a low extinction coefficient, short radiative lifetimes, and correspondingly low fluorescent yields. The absorption bands of the pigments bound in the native protein, on the other hand, are comparatively narrow and increased up to 5-fold in intensity. They are highly fluorescent and have lifetimes increased by up to 4 orders of magnitude. All this is reflective of an increased rigidity of the bilin and the presence of only a few conformers.^{36–38} Protonation of the bilin chromophores in the biliproteins by aspartate residues close to the two central nitrogens is an additional source for increased absorption in the native phycobiliproteins.³⁹ In contrast to the high phototoxicity of chlorophyll, there is currently no evidence that biliproteins can generate singlet oxygen, either in their free state or integrated into the native protein, which explains why carotenoids are not needed for photoprotection in PE545.

Previous spectroscopic studies on PE545, including circular dichroism, fluorescence excitation anisotropy, and 2-photon excitation,^{11,29,40–42} have speculated on energy-transfer mechanisms and have suggested models of excitation flow but are based almost entirely on steady-state measurements. Recently, an improved model has been proposed by Doust et al.,¹⁰ based on the ultrahigh-resolution crystal structure, in combination with steady-state and ultrafast spectroscopic data and additional quantum chemical calculations. In that model, excitation energy is funneled from four peripheral pigments ($\beta 158, \beta 82$) into the central chromophore dimer ($\beta 50/\beta 61$). Those chromophores, in turn, transfer the excitation energy to the red-absorbing molecules located at the periphery of the complex. A final resonance-energy transfer step was suggested to sensitize just one of the $\alpha 19$ bilins, by way of a Förster-type mechanism, on a time scale of 22 ps.

We report here ultrafast transient absorption measurements. Even though spectral congestion is significant, the results enable us to visualize the evolution of the energy-transfer dynamics in PE545 over the entire spectral range. Our analysis exposes the important role of the central dimer in capturing and redistributing excitation energy within the PE545 complex.

Materials and Methods

Sample Preparation. Algal cells of *Rhodomonas* species were cultivated, and PE545 was isolated and concentrated according to a method described previously.¹⁰ Samples of PE545 were kept frozen at -80 °C in the dark until required for experimental use. Before measurements were taken, the sample was diluted with buffer solution to the desired optical density. The buffer solution was made from 0.050 M MES (2-[*n*-morpholino] ethanesulfonic acid, purchased from Sigma) in deionized water. The pH was adjusted to 6.5 using concentrated NaOH solution, and 1 mM NaN_3 (Sigma) was added. For the 77 K temperature measurements, the sample was diluted to the appropriate optical density in buffer + 70% (w/v) glycerol.

Laser Setup. The dispersed pump–probe setup has been described in detail earlier.^{43,44} The basis of the system is a 1-kHz

amplified Ti/sapphire system (BMI) delivering 450- μ J, 60-fs, 800-nm pulses. The excitation pulses were generated with a home-built noncollinear optical parametric amplifier that is pumped by the second harmonic of the amplified 800-nm light. The white-light continuum, used for broad-band probing, was generated by focusing a weak 800-nm beam into a slowly translating CaF₂ crystal. Reflective optics steered and focused the probe beam, reducing the group velocity dispersion to \sim 200 fs over 450–650 nm. The relative polarization of the pump and probe pulses was set to magic angle (54.7°), and the pump beam spot size at the focus was \sim 100 μ m. The collected data have a 1-nm wavelength resolution and an average noise level of $<$ 1 mOD.

Room-temperature measurements were performed with the sample of optical density of 0.4 per mm at the absorption maximum flowing in a 1-mm flow cell that was rapidly translated with a small amplitude shaker. The 77 K measurements were performed with the PE545 sample held in a 1-mm static cell, which was mounted within an Oxford liquid-nitrogen Dewar cryostat (Optistat-DN). To remove interfering effects (and degradation) from exciting small sample volumes during the experiment, the cell was rapidly translated with the aid of a home-built insert.⁴⁵ For both 530- and 485-nm excitation wavelengths, a probe window between 400 and 700 nm was measured, up to a maximum delay of 200 ps. Pump intensities of 30–80 nJ were used, corresponding to excitation densities of 10^{14} – 10^{15} photons/pulse/cm². At these excitation densities, it is estimated that between 3 and 15% of the complexes are excited, and using the Poisson distribution⁴⁶

$$P(k) = \frac{N^k \exp(-N)}{k!} \quad (1)$$

$P(k)$, the probability of k excitations per complex, can be calculated. N is the average number of excitations per complex, and we find that there is a maximum probability of 13%, 1%, and 0.05% of finding 1, 2, or 3 excitations per complex, respectively.

Data Analysis. The time-gated spectra were analyzed with a global fitting program that has been previously described.⁴⁷ Evolution-associated difference spectra (EADS) were estimated using a sequential, irreversible model $A \rightarrow B \rightarrow C$, and so forth, with increasing lifetimes. This picture enables us to visualize clearly the evolution of the excited states in the system, although the EADS need not be associated with “pure states”. This is because the number of kinetic components that can be estimated from the experimental data does not equal the number of pigments, which is caused by a combination of a lack of time resolution, by time constants having approximately the same value, and by pigments having approximately the same spectra and hence strong spectral overlaps. Hence the analysis reveals only a few kinetic components, even though there are many more energy-transfer processes likely occurring between the eight bilins in PE545. However, the unidirectionality of the kinetic processes is reasonable, especially for the 77 K data as uphill energy transfer can be ignored at this temperature. The kinetic components then reflect the processes occurring between groups of pigments, characterized by unidirectional energy-transfer rates. The instrument response function, fitted with a Gaussian profile, had full width at half-maximum (fwhm) values of 100–120 fs. The probe pulse dispersion was fitted to a third-order polynomial function of the wavelength, and the obtained parameters agreed very well with those found for several other experiments performed under similar conditions.

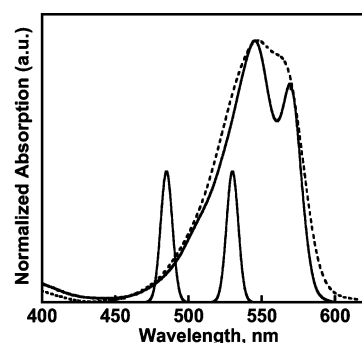


Figure 3. Room-temperature (dashed) and 77 K (solid) absorption spectra of PE545. Also shown are the excitation pulses used in the transient absorption measurements centered on 530 and 485 nm.

Spectral Modeling. We have attempted to get a better understanding of the spectral positions of the bilins in PE545 by generating exciton eigenvalue spectra, dressed with Gaussians, to match closely the absorption line shapes at room temperature and 77 K and to qualitatively resemble the room-temperature CD spectrum. Accurate fitting of CD spectra of phycobiliproteins is challenging because phycobilin chromophores are chiral; thus, in addition to the circular dichroism arising from the transition dipole–dipole interaction, there is an intrinsic contribution to the CD spectrum that cannot be incorporated into simple calculations.^{15,48,49} The electronic coupling values were calculated from the interpigment distances and orientation factors taken from Table 5 of ref 10, and they were used to generate the system Hamiltonian, where the spectral positions were taken to be 539 nm for all PEB bilins and 564 and 567 nm, respectively, for the two DBV bilins. The DBV bilin bands were found to require an increased oscillator strength compared to the PEB bilins, which is in agreement with the quantum mechanical calculations reported previously.¹⁰ To model the 77 K spectrum, the Gaussian line shapes were narrowed by reducing σ by 27%.

The Hamiltonian was diagonalized and the absorption spectra were generated using the following equation:

$$\mu_K^2 = \sum_{i,j=1}^N \mu_i \mu_j (\hat{\mu}_i \cdot \hat{\mu}_j) U_{iK} U_{jK} \quad (2)$$

where N represents the number of interacting bilins (eight for PE545), μ_i is the strength in Debye of transition in the i th molecule, $\hat{\mu}_i$ is the unit vector in the direction of that transition, and U_{iK} is the i th element of the eigenvector for the K th exciton state.

Results

The organization of the pigments in PE545 is shown in Figure 1, where the stacking orientation of the terminal pyrrole units of the central β 50/61 pair in the middle of the figure is clear to see. The absorption spectra at room temperature and 77 K are shown in Figure 3, along with the excitation pulse spectra used in the transient absorption measurements. The six PEB bilins cover the spectrum from 470 to 560 nm, and the red-shifted DBV bilins are responsible for the red shoulder in the room-temperature spectrum and for the red peak at 77 K. The emission band at 579 nm (not shown) is attributed to one of the DBV bilins only, and is thus relatively narrow. The excitation spectrum corresponds closely to that of the absorption line shape. The excitation wavelengths were chosen to investigate energy migration in PE545 by exciting at the blue edge

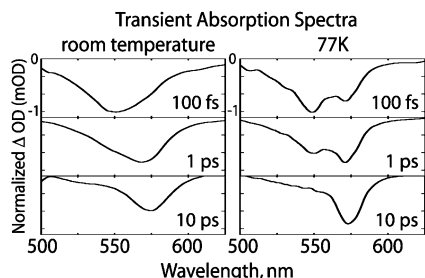


Figure 4. Normalized room-temperature and 77 K transient absorption spectra at 100 fs, 1 ps, and 10 ps, respectively. The excitation wavelength is 485 nm. The red shifting of the induced bleach from 550 to 575 nm is evident.

TABLE 1: Energy-Transfer Times Estimated from the EADS Spectra^a

temperature, K	excitation wavelength, nm	T1, ^b fs	T2, ^c fs	T3, ^c ps	T4, ps	T5, ns
			red	blue	green	black
298	485	25	250	1.84	23.5	1
298	530	25	250	1.84	16.4	>1
77	485	25	960	3.0	30	>1
77	530	25	960	3.0	17.7	>1

^a Energy-transfer times were estimated from the global analysis of the transient absorption data at the indicated excitation wavelengths and temperatures. ^b T1 is arbitrarily set to 25 fs and represents dynamics that are faster than the time-resolution of the experiment. ^c For T2 and T3, the time scales for 485- and 530-nm excitation were linked in the simultaneous analysis at a given temperature, see text for further details. The colors indicated for T2, T3, T4, and T5 correspond to the EADS lifetimes in the spectra in Figures 5 (298 K) and 6 (77 K).

of the absorption (485 nm) and at the estimated spectral location of the higher exciton state of the dimer (530 nm). The transient spectra consist of a positive peak centered around 450 nm due to excited-state absorption (ESA) and negative signals between 480 and 640 nm reflecting contributions of the ground-state bleach (BL) and stimulated emission (SE). Beyond 640 nm, there is more ESA contribution to the transient absorption spectra. The buildup of both BL/SE and ESA is instantaneous, followed by the spectral changes governed by relaxation and energy-transfer dynamics. The red-shifting of the BL/SE signals as energy-transfer dynamics occur in PE545 are shown in the transient spectra in Figure 4.

Each data set was globally analyzed using an evolutionary kinetic scheme. Five lifetimes were needed to obtain a satisfactory fit of all data sets (see Table 1). The first lifetime was arbitrarily set to 25 fs because it cannot be precisely estimated from these data with this instrument response function width, but it is evidently very short. Its EADS (not shown) represents a mixture of coherent artifacts, a 3600-cm^{-1} Raman band, and possible ultrafast, sub pulse-width processes; it will not be discussed further here. Since the next two lifetimes were very close for the two excitation wavelengths, they were linked in a simultaneous analysis, implying that most likely they represent the same process(es). They were estimated to be 0.25 and 1.84 ps at room temperature, and 0.96 and 3.0 ps at 77 K. The next lifetime, which is in the range 18–30 ps, could not be linked. The lifetime of the long-lived state was larger than 1 ns (the fluorescence lifetime of the emitting α 19 bilin is 2.5 ns at room temperature¹), but could not be estimated accurately due to the limited time window of 200 ps. Four EADS are shown in Figure 5 (room temperature) and Figure 6 (77 K), where solid lines are for 485-nm excitation and the dashed lines for 530-nm excitation. The first EADS representing the first 25-fs lifetime are not shown. The 77 K data sets provided excellent spectral

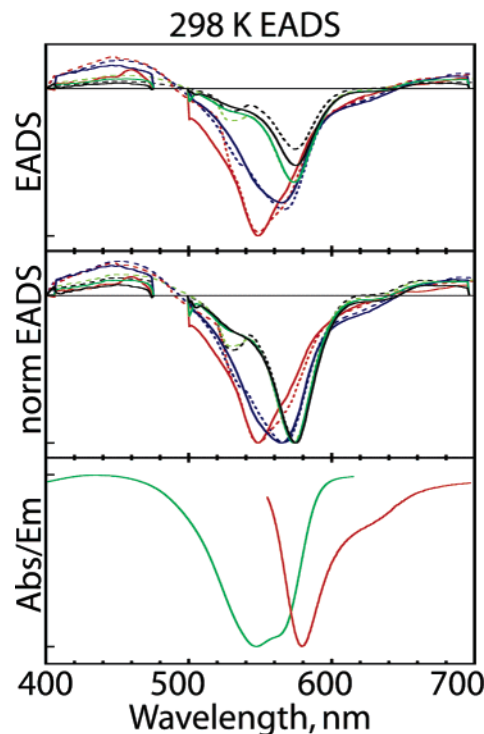


Figure 5. Evolution-associated difference spectra (EADS) that are obtained from fitting the room-temperature transient absorption data for PE545 with 485-nm (solid) and 530-nm (dashed) excitation. The first EADS, containing the coherent artifacts, has been omitted. The color order is the following: red, blue, green, black. The associated lifetimes are collated in Table 1. The bottom panel shows the absorption and emission spectra of PE545 at room temperature.

resolution due to the narrowing of the bands, allowing for well-interpretable EADS.

At both room temperature and 77 K and for both excitation wavelengths, we observe the excitation to be localized on either the lower dimer state or one of the DBV bilin(s) within 50 fs of excitation. Thus, the dynamics of energy transfer and exciton relaxation occur within the laser pulse duration and cannot be resolved with the time resolution of the experiment. A target analysis including various branchings in the kinetic scheme was attempted, as was increasing the number of lifetimes, but due to the spectral congestion it was not possible to accurately estimate more than four EADS shapes reliably.

a. EADS Interpretation. After excitation, the transient spectra transform very rapidly on a time scale set to be 25 fs into the red EADS, where most of the excitation is located on the lowest exciton state of the dimer and the other PEB bilins (548 nm for room temperature and 550 nm for 77 K). It is interesting to note the subtle differences in this initial red EADS, where 530-nm excitation (dashed line) promotes a greater initial population of the red-most pigments than does 485-nm excitation (solid line), as evidenced by the shoulder at 570 nm. This is especially evident at 77 K. This is so because the red bilins can be directly excited by 530-nm light as their absorption extends into this region, but they cannot be excited directly by 485-nm excitation. The initial red EADS transforms into the blue EADS in 250 fs at room temperature and about a picosecond at 77 K. It is clear to see that though most of the excitation has now reached the red DBV bilins, there is still some residual excitation of the 550-nm state, especially at room temperature, where the red-shift is not as significant as at 77 K.

The blue EADS then transforms into the green EADS in under 2 ps at room temperature and in 3 ps at 77 K, which is in

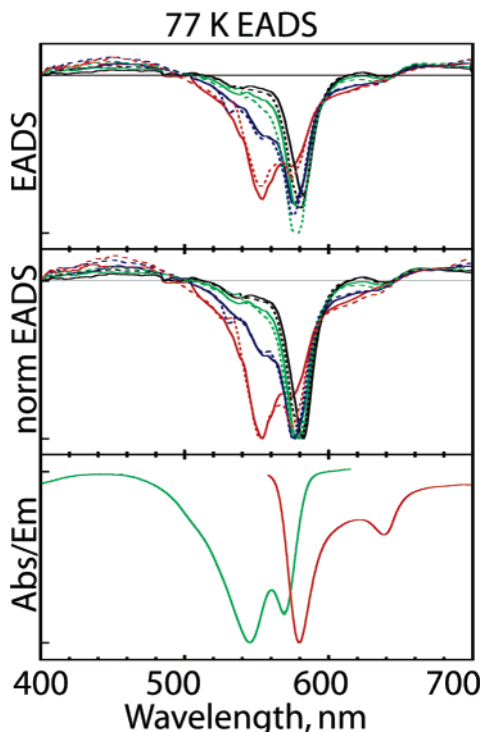


Figure 6. Evolution-associated difference spectra (EADS) that are obtained from fitting the 77 K transient absorption data for PE545 with 485-nm (solid, black) and 530-nm (dashed) excitation. The first EADS, containing the coherent artifacts, has been omitted. The color order is the following: red, blue, green, black. The associated lifetimes are collated in Table 1. The bottom panel shows the absorption and emission spectra of PE545 at 77 K.

agreement with the depletion of excitation of the 550-nm state, meaning all the excitation is now located on the red DBV bilins. At room temperature, this also corresponds to a decrease in the total integrated BL/SE signal as the excitation is funneled from 6 PEB bilins to only two, and then one final trap bilin. A red-shift of the BL/SE maximum to 574 nm is seen. At 77 K, the pulse intensity was lower, and therefore the number of excitations of the complex was fewer; hence, the decrease of the integrated BL/SE signal is less profound.

For both blue and green, dashed and solid, the EADS are similar, indicating that, although the excitation wavelengths are different, by 250 fs after excitation at room temperature and 960 fs at 77 K, the excitation energy has accumulated on the same set of bilins, which highlights how well tuned the system is to harvesting light across the 485–550-nm range. This equilibration of the excitation energy is remarkably rapid. The final energy-transfer time, which corresponds to the green-to-black EADS, is dependent on the wavelength of excitation and involves a final red shift to 575 nm. In this step, all the energy is accumulated on the red-most DBV bilin with energy-transfer times of 23.5 ps (485-nm excitation) and 16.4 ps (530 nm) at room temperature and 30 ps (485 nm) and 18 ps (530 nm) at 77 K. It is faster at 530-nm excitation because the number of excitations per complex is slightly greater at this excitation wavelength. Nevertheless, we have ruled out annihilation as the dominant mechanism as only 1% of the complexes have been estimated to be doubly excited. If multiple excitations in one PE545 complex converge on the same red-most DBV bilin, the total integrated BL/SE signal of the red DBV bilins decreases between the green and black EADS, which is seen to be minimal for the 485-nm, 77 K measurement. We believe that the value of 30 ps represents the best estimation of this energy-transfer time scale as the pump intensity (which were normalized for

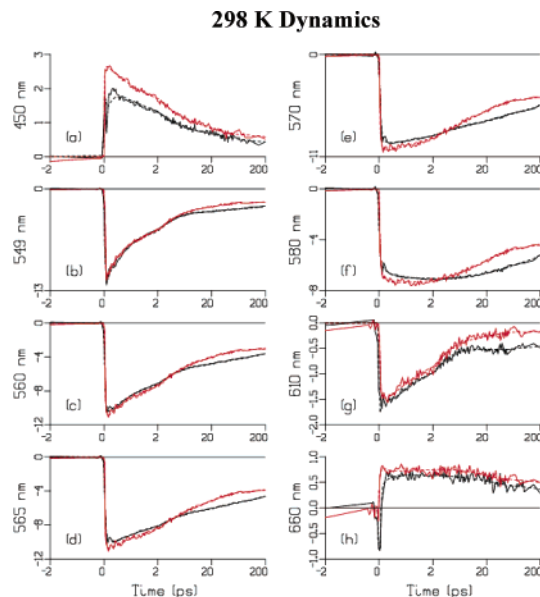


Figure 7. (a)–(h) Kinetic traces at various probe wavelengths at room temperature. Excitation wavelengths are 485 nm (solid, black) and 530 nm (solid, red), with the dashed lines the fit from the EADS analysis. The time axis is linear from -2 to 2 ps, logarithmic thereafter.

all data sets in the analysis) was lowest for the 485-nm, 77 K scan, and the EADS is annihilation-free. The energy-transfer times faster than 30 ps could be partially due to annihilation, or perhaps a photoinduced isomerization mechanism of the emitting bilin, leading to the 644-nm BL/SE signal. At this stage, we are not entirely sure. However, although these processes may be occurring and are of interest for future study, the dominant processes are those of energy transfer.

The black EADS decay with time constants larger than 1 ns, which is much longer than the measuring time window (200 ps), represent the lifetime of the emitting bilin which has previously been measured to be 2.5 ns at room temperature.¹ It is worth noting that the relative intensity of the BL/SE band at 575 nm compared to the 550-nm band is much greater at 77 K, which can partly be explained by less annihilation at 77 K, but is most likely due to an increase in the fluorescence quantum yield of PE545 at lower temperatures as has also been seen in other biliproteins.^{8–10}

b. Kinetic Traces. The kinetic traces recorded at room temperature and 77 K are shown in Figures 7 and 8, respectively. A range of wavelengths were chosen to highlight BL/SE and ESA features, the energy-transfer kinetics, as well as to show the EADS analyses of the data. In the figures, the black traces are for the 485-nm excitation data, and the red traces represent 530-nm excitation.

In (a), the traces at 450 nm correspond to the ESA region at the blue edge of the ground-state absorption band. The intensity of the red (530 nm) traces is greater because the absorption of PE545 at 530 nm is greater than at 485 nm; however, both traces decay according to similar kinetic lifetimes and have a DBV-to-DBV energy-transfer character. The 550-nm traces (b) correspond to the center of the lowest exciton band of the central dimer. After the near instantaneous bleach of this band, it recovers as the excitation is transferred to the more red DBV bilins, the rates being equal regardless of the excitation wavelength. That the BL/SE recovery happens on more than one time scale is clear from the traces, which show multiple regions of decay kinetics and also highlight the fact that plenty of excitation still resides at this wavelength after the initial decay dynamics.

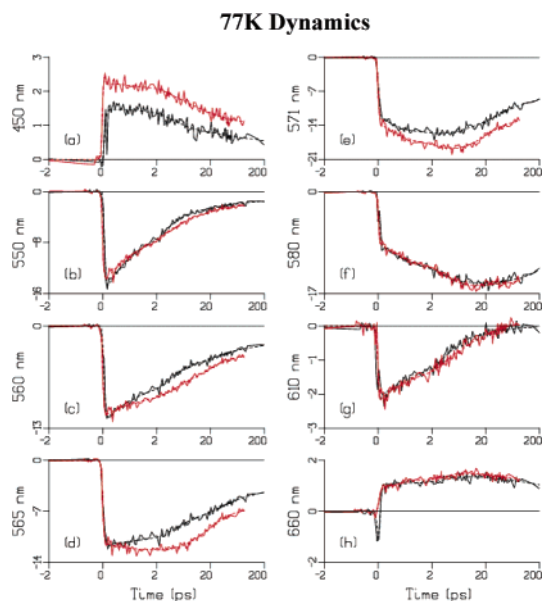


Figure 8. (a)–(h) Kinetic traces at various probe wavelengths at 77 K. Excitation wavelengths are 485 nm (solid, black) and 530 nm (solid, red), with the dashed lines the fit from the EADS analysis. The time axis is linear from -2 to 2 ps, logarithmic thereafter.

The 560- and 565-nm traces in (c) and (d), respectively, correspond to the region in the spectrum between the PEB and DBV bilins. The BL/SE recovery at this wavelength is slower than at 550 nm because the kinetics of the signal is now a combination of BL/SE recovery of the 550-nm band and the in-growing of the DBV BL/SE. At 565 nm, the room-temperature traces are quite different from the 77 K traces due to the difference in widths of the bilin absorption bands at these temperatures. At room temperature, after ~ 3 ps the recovery of the signal is faster for the 530-nm excitation scan at this excitation wavelength. At 77 K, it is clear to see in the 560- and 565-nm bands that the BL/SE is greater for 530-nm excitation, although the kinetics of recovery, which represents the energy transfer to the red-most bilin, are very similar. The traces at 565 nm in particular are in the spectral region between the PEBs and DBVs; hence, for the first few picoseconds, the BL/SE signal does not change as excitation is transferred from the PEB bilins to the two DBV bilins.

The 570-nm (e) and 580-nm (f) kinetic traces represent the growth and decay of BL/SE for the DBV bilins. At room temperature, the instantaneous BL/SE signal is slightly greater for the 530-nm excitation traces, which makes sense as more of the DBV bilins will have been excited. It can be seen that the time constants of the in-growing of the BL/SE signal are significantly faster at room temperature when compared to 77 K. At 580 nm, it is clear to see that the excitation is reaching the red-most bilin as the BL/SE signal increases, stabilizes, and then decays with the fluorescence lifetime.

At 77 K, 610 nm is close to an isosbestic point for the red-most DBV bilin data, where its ESA and SE cancel (see the black EADS in Figure 6). Therefore, the traces at 610 nm (g) represent the decay of the SE of the PEB bilins, which is complete in under 20 ps at room temperature and around 20 ps at 77 K concurrent with population decay of the PEB bilins. The kinetics of the ESA region at 660 nm is shown in trace (h), which shows that the nearly instantaneous rise in signals decays very slowly throughout the 200 ps during which data were taken, suggesting that this feature is related to the red-most DBV bilin, which has a 2.5-ns lifetime at room temperature.

Discussion

The previously published model of energy-transfer dynamics in PE545, based on transient grating results and quantum chemical calculations, suggested that the four PEB bilins absorbed light in the 485–535-nm range, the dimer at 545 and 553 nm, and the DBV bilins at 565 and 572 nm, respectively.¹⁰ It was also thought that all the excitation from the peripheral PEB bilins was trapped by the dimer in the core of the complex and directed on to the DBV bilins. Because it was impossible to assign energy-transfer times to specific kinetic processes on the basis of the transient grating data, and the role of the dimer was known to be important, but not well understood, broadband transient absorption measurements were performed. The data presented in this paper allow for a significant improvement to the model as the combination of the EADS analyses and calculated spectra provide a clear account of the spectral positions and energy-transfer times from groups of bilins.

A summary of the observed time scales and their temperature and excitation-wavelength dependence are given in Table 1. The room-temperature time scales are faster than at 77 K, owing to more favorable spectral overlap factors. The fourth EADS time scale (T4 in Table 1), which amounts to the DBV \rightarrow DBV energy-transfer step, is minimal for the 77 K, 485-nm experiment. This energy-transfer step is thus considered to be close to 30 ps, which corresponds well with the room-temperature time scale measured by transient grating.¹⁰ Earlier estimates of this energy-transfer step, which can be obtained using the Förster equation⁵⁰ in the weak coupling limit, gave an energy-transfer rate of 22.1 ps.¹⁰ It is now thought, however, that the dipole strength is less than 12 D, reducing the coupling strength and subsequently the predicted energy-transfer rate. At 77 K, the energy-transfer steps (T2, T3, T4 from Table 1) do not decrease significantly, compared with room-temperature, illustrating the optimized spectral overlap between the bilins in PE545.

As stated in the Materials and Methods section, we have attempted to reproduce the room-temperature and 77 K absorption spectra with a concurrent qualitative reproduction of the CD spectrum. The calculation shows that the dimer states are split into low- and high-energy bands at 531 and 549 nm, respectively, and the other PEB bilins maintain a spectral position of 539 ± 1.5 nm. The DBV bilins maintain their spectral positions of 564 and 567 nm, as shown in Figure 9. The two DBV bilins are essentially monomeric, and the four nondimer PEB bilins are somewhat delocalized in the absence of electron–phonon coupling. In other words, the suggestion from the earlier paper that the spectral positions of the bilins could be found and proposed by the second derivative of the absorption spectrum has been found to be inaccurate; instead, the spectral positions are likely to be much closer together. That greatly enhances spectral overlap between all the bilins, with the vibronic tail responsible for the absorption stretching to 450 nm. Hence, it is now possible to elucidate a realistic kinetic model of energy transfer in PE545, taking into account the kinetic components that the transient absorption measurements have illustrated, the calculated spectral positions and couplings of the bilins, and estimates of spectral overlap factors from the generated deconvoluted absorption spectra.

The dynamics of the highly coupled central dimer were unresolvable in these measurements. That is not surprising given that for systems such as the reaction center special pair, LH2 or the allophycocyanin trimer, the exciton relaxation dynamics are of the order of tens of femtoseconds. For example, the dynamics observed following direct excitation of the P₊ upper exciton absorption band of the photosynthetic reaction center

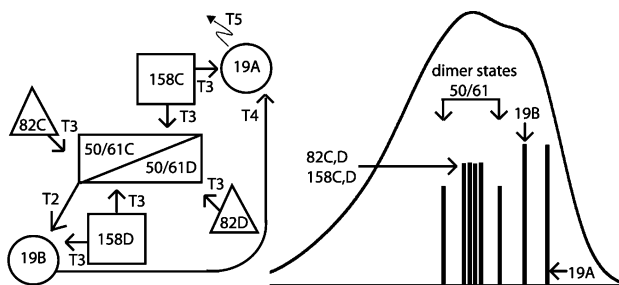


Figure 9. A model of energy transfer in PE545 (left panel), and spectral positions of the bilins in PE545 (right panel). Excitation is funneled from the peripheral PEB bilins to the central dimer from where it is transferred to the DBV bilins. Rates T2, T3, and T4 refer to the EADS time scales of Table 1, and T5 is the fluorescence lifetime of the emitting bilin. See discussion for further explanations.

of *Rb. sphaeroides* suggests that internal conversion between the excitonic states of P occurs with a 65-fs time constant.^{14,51,52} Interexciton-state relaxation in the dimer in allophycocyanin occurs on a ~ 30 -fs time scale,^{15,16} concurrent with a red-shift to the lower exciton state. The fact that exciton states are involved means that there is a possibility that ESA in the 450–550-nm region might arise from transitions populating doubly excited exciton states, making the transient absorption BL/SE signal appear weaker in the 500–525-nm region. This has been seen and described in the highly coupled and delocalized bacteriochlorophyll-*a* ring system of the B850 band in LH2, where in the transient absorption spectra, a positive peak due to ESA is evident at 835 nm.^{53–57} Similar results have been reported for the purple bacteria reaction center.^{52,58,59} However, the ESA in the present experiment contains slow DBV \rightarrow DBV recovery kinetics, so it is hard to judge to what extent the dimer plays a role in these signals.

Ultimately from the dimer trap, the excitation is transferred from the center of the protein to the periphery, where the DBV bilins are responsible for taking the excitation and that from the other PEB bilins and efficiently passing it on to the chlorophylls in the membrane. Besides the sub pulse-width dynamics of the dimer, some of the predicted energy-transfer rates from the $\beta 158$ and $\beta 82$ bilins to the lowest exciton state of the dimer and DBV bilins are ultrafast and not directly detectable in PE545. To be able to calculate such electronic energy-transfer dynamics, a generalization of Förster's theory is required. Such a theory has been developed and applied to calculating the B-to-P energy-transfer times in the bacterial photosynthetic reaction center.^{51,60–63} It was found that B-to-P energy-transfer times were on the order of 90 fs in *Rps. viridis* and 180 fs in *Rb. sphaeroides*.⁵⁴ The temperature dependence of these energy-transfer rates was small despite the large change in spectral overlap, precluding the Förster mechanism, which depends on spectral overlap, from playing a major role in the energy/excitation process.⁶⁴ Such an analysis is the subject of future work.

Figure 9 highlights the dynamic processes in PE545. The bilins have been divided into three groups; the central dimer bilins ($\beta 50/\beta 61$), the PEB bilins ($\beta 158, \beta 82$), and the DBV bilins ($\alpha 19$). The first process that occurs at sub pulse-width time resolution is the internal conversion from the high to the low exciton state of the central dimer, which is part of the T1 set at 25 fs. From the lowest exciton state, the energy transfers to the blue-most DBV bilin in around 250 fs, as deduced from T2 of the EADS analysis. T3 from the EADS analysis is a combination of a number of energy transfers; as mentioned earlier, due to very similar time scales and spectral features, it is difficult to

separate some processes between the eight bilins in PE545 and hence they are grouped together as such. In this case, it is predicted that T3 encompasses all of the following energy transfers: the $\beta 158$ and $\beta 82$ bilins to the lowest exciton state of the central dimer ($\beta 50/\beta 61$ C), as well as direct energy transfer of $\beta 158$ D to $\alpha 19$ B and $\beta 158$ C to $\alpha 19$ A, which is arbitrarily chosen to be the DBV bilin responsible for emission. Due to the symmetry of PE545, this assumption is a fair one. The final energy-transfer step results in all the excitation ending up on the final emitting DBV bilin. It is also concluded that there is no energy transfer among the $\beta 158$ and $\beta 82$ bilins. The existence of the central dimer in PE545 is important in this organism as it relies on just two bilin types to cover the same part of the spectrum, which in cyanobacteria and red algae is covered by multiple proteins and bilins in the phycobilisome structures. The dimer in PE545 expands spectral coverage and ensures highly efficient and ultrafast trapping of energy, and also mediates the ensuing transfer of this excitation to the red DBV bilins.

Besides the energetic dynamics within PE545, it is of course also important to consider what happens to the excitation once it reaches the emitting $\alpha 19$ bilin. Even though it has been concluded that binding of PE545 to the thylakoid membrane is not essential for efficient energy transfer to the integral membrane chlorophyll-*a* containing complexes associated with PS-II,¹⁰ it is still unclear how this energy-transfer step occurs. It is believed that some of the PE545 proteins will have a loose association with the membrane, while other uncoupled proteins transfer their excitation in a stochastic mechanism to those closer to the membrane. In PBS, the binding of linker polypeptides to phycobiliproteins has been seen to red-shift the fluorescence by up to 10 nm,⁸ which, if such spectral changes occur upon association of the PE545 with the membrane, would increase the spectral overlap between the $\alpha 19$ bilin emission and acceptor chlorophyll. The lumen is believed to be around 300 Å in width, allowing up to seven PE545 proteins to squeeze into the luminal space. The observation of fluorescence decay times for PE545 (110 ps) and PE566 (100 ps), which are faster than for PC645 (250 ps) in whole cells at 77 K, despite a 4.3- or 2.5-fold decrease in spectral overlap with chlorophyll-*a*, provides some support for chlorophyll-*c* functioning as an intermediate in the PE-containing species.¹³ Comparisons with PCP are strong, as both proteins act as light-harvesting antenna complexes in the lumen, and both have a red \rightarrow red final energy-transfer step of the order of a few tens of picoseconds.²³ Other similarities are the distance the final energy-transfer step undergoes and the accurate prediction of this energy transfer by way of the Förster mechanism. What happens to the excitation in both these proteins could well be very similar.

Conclusions

In conclusion, we have performed transient absorption spectroscopy with 120-fs time resolution on phycoerythrin 545 of a cryptophyte algae. We have been able to develop an improved kinetic model for the exciton dynamics of PE545. Specifically, internal conversion of the dimer occurs faster than the time resolution of the experiment, and energy transfer from the lowest exciton state of the dimer to one of the DBV bilins was concluded to occur in 250 fs at room temperature and in 960 fs at 77 K. Energy-transfer dynamics involving the $\beta 158$, $\beta 82$, $\beta 50/61$ bilins to the $\alpha 19$ DBV bilins occurred on an estimated time scale of 1.84 ps at room temperature and 3 ps at 77 K. The third time scale, involving energy transfer between the two DBV bilins was estimated to be ~ 30 ps. The energy-transfer time scales were shown to be relatively independent of

excitation wavelength, meaning that PE545 is a highly optimized system able to harvest light across 450–600 nm of the energy spectrum. The central dimer in PE545 plays a crucial role in the efficient functioning as a light-harvesting protein by expanding the cross section of absorption of the protein, structurally by acting as a central intermediary trap ensuring ultrafast and directional energy transfer and kinetically, as the internal conversion and subsequent red-shift of the excitation is extremely fast.

Acknowledgment. We gratefully acknowledge the following sources for funding: Natural Sciences and Engineering Council of Canada, Canada Foundation for Innovation and the Ontario Innovation Trust, University of Toronto and the Research Corporation. D.S.L. is grateful to the Human Frontier Program Organization for providing financial support with a long-term fellowship. G.D.S. is an Alfred P. Sloan fellow. The research of VU-Biophysics is supported by The Netherlands Organization of Scientific Research (NWO) via the foundation of Earth and Life Sciences (ALW).

References and Notes

- Wilk, K. E.; Harrop, S. J.; Jankova, L.; Edler, D.; Keenan, G.; Sharples, F.; Hiller, R. G.; Curmi, P. M. G. *Proc. Natl. Acad. Sci. U.S.A.* **1999**, *96*, 8901.
- Gantt, E. *Int. Rev. Cyt.* **1980**, *66*, 45.
- MacColl, R.; Guard-Friar, D. In *Phycobiliproteins*; CRC Press: Boca Raton, FL, 1987.
- Morschel, E.; Rhiel, E. In *Electron Microscopy of Proteins*, 6th ed.; Harris, J. R., Horne, R. W., Eds.; Academic Press: New York, 1987; p 209.
- Glazer, A. N. *Biochim. Biophys. Acta* **1984**, *768*, 29.
- Homoelle, B. J.; Edington, M. D.; Diffey, W. M.; Beck, W. F. *J. Phys. Chem. B* **1998**, *102*, 3044.
- MacColl, R.; Malak, H.; Gryczynski, I.; Eisele, L. E.; Mizejewski, G. J.; Franklin, E.; Sheikh, H.; Montellse, D.; Hopkins, S.; MacColl, L. C. *Biochemistry* **1998**, *37*, 417.
- Glazer, A. N. *Annu. Rev. Biophys. Biophys. Chem.* **1985**, *14*, 47.
- Yamazaki, I.; Mimuro, M.; Murao, T.; Yamazaki, T.; Yoshihara, K.; Fujita, Y. *Photochem. Photobiol.* **1984**, *39*, 233.
- Doust, A. B.; Marai, C. N. J.; Harrop, S. J.; Wilk, K. E.; Curmi, P. M. G.; Scholes, G. D. *J. Mol. Biol.* **2004**, *344* (1), 135.
- Spear-Bernstein, L.; Miller, K. R. *J. Phycol.* **1989**, *25*, 412.
- Gantt, E. In *Biochemistry and Physiology of Protozoa*, 2nd ed.; Levandowsky, M., Hutner, S. H., Eds.; Academic Press: New York, 1979; Vol. 1, p 121.
- Bruce, D.; Biggins, J.; Steiner, T.; Thewalt, M. *Photochem. Photobiol.* **1986**, *44*, 519.
- Jordanides, X. J.; Scholes, G. D.; Fleming, G. R. *J. Phys. Chem. B* **2001**, *105*, 1652.
- Edington, M. D.; Riter, R. E.; Beck, W. F. *J. Phys. Chem. B* **1996**, *100*, 14206.
- Edington, M. D.; Riter, R. E.; Beck, W. F. *J. Phys. Chem.* **1995**, *99*, 15699.
- Kasha, M.; Rawls, H. R.; Ashraf El-Bayoumi, M. *Pure Appl. Chem.* **1965**, *11*, 371.
- Renger, T.; May, V. *J. Phys. Chem. A* **1998**, *102*, 4381.
- Vulto, S. I. E.; de Baat, M. A.; Neerken, S.; Nowak, F. R.; van Amerongen, H.; Amesz, J.; Aartsma, T. J. *J. Phys. Chem. B* **1999**, *103*, 8153.
- Koolhaas, M. H. C.; van der Zwan, G.; Frese, R. N.; van Grondelle, R. *J. Phys. Chem. B* **1997**, *101*, 7262.
- Jimenez, R.; van Mourik, F.; Young Yu, J.; Fleming, G. R. *J. Phys. Chem. B* **1997**, *101*, 7350.
- Scholes, G. D.; Fleming, G. R. *J. Phys. Chem. B* **2000**, *104*, 1854.
- Ilagan, R. P.; Shima, S.; Melkozernov, A.; Lin, S.; Blankenship, R.; Sharples, F. P.; Hiller, R. G.; Birge, R. R.; Frank, H. A. *Biochemistry* **2004**, *43*, 1478.
- Wedemayer, G. J.; Kidd, D. G.; Glazer, A. N. *Photosynth. Res.* **1996**, *48*, 163.
- Martin, C. D.; Hiller, R. G. *Biochim. Biophys. Acta* **1987**, *923*, 88.
- Hiller, R. G.; Martin, C. D. *Biochim. Biophys. Acta* **1987**, *923*, 98.
- Rowan, K. S. In *Photosynthetic Pigments of Algae*; Cambridge University Press: Cambridge, 1989.
- Hill, D. R. A.; Rowan, K. S. *Phycologia* **1989**, *28*, 455.
- Sidler, W. A. In *Advances in Photosynthesis*, Vol. 1, *The Molecular Biology of Cyanobacteria*; Bryant, D. A., Ed.; Kluwer Academic Publishers: Dordrecht, The Netherlands, 1994; p 139.
- Lichtle, C.; Juspín, H.; Duval, J. C. *Biochim. Biophys. Acta* **1980**, *591*, 104.
- Lichtle, C.; Duval, J. C.; Lemoine, Y. *Biochim. Biophys. Acta* **1987**, *894*, 76.
- Cheng, L.; Jiang, L. *Chin. Chem. Lett.* **1991**, *2* (7), 589.
- Borisov, A. Y. *Photosynth. Res.* **1989**, *20*, 35.
- Huber, R. *EMBO J.* **1989**, *8*, 2125.
- Scheer, H. Book of Abstracts, 13th International Congress of Photosynthesis, Montreal, 2004.
- Braslavsky, S. E.; Holzwarth, A. R.; Schaffner, K. *Angew. Chem., Int. Ed. Engl.* **1983**, *22*, 656.
- Scheer, H.; Kufer, W. Z. *Naturforsch., C: Biosci.* **1977**, *32C* (7–8), 513.
- MacColl, R.; Guard-Friar, D.; Ryan, T. J. *Biochemistry* **1990**, *29*, 430.
- Kikuchi, H.; Wako, H.; Yura, K.; Go, M.; Mimuro, M. *Biophys. J.* **2000**, *79*, 1587.
- MacColl, R.; Lam, I.; Choi, C. Y.; Kim, J. J. *Biol. Chem.* **1994**, *269*, 25465.
- MacColl, R.; Eisele, L. E.; Dhar, M.; Ecuyer, J. P.; Hopkins, S.; Marrone, J.; Barnard, R.; Malak, H.; Lewitus, A. J. *Biochemistry* **1999**, *38*, 4097.
- MacColl, R.; Eisele, L. E.; Marrone, J. *Biochim. Biophys. Acta* **1999**, *1412*, 230.
- Gradinaru, C. C.; van Stokkum, I. H. M.; Pascal, A. A.; van Grondelle, R.; van Amerongen, H. *J. Phys. Chem. B* **2000**, *104*, 9330.
- Larsen, D. S.; Vengris, M.; van Stokkum, I. H. M.; van der Horst, M.; de Weerd, F. L.; Hellingwerf, K. J.; van Grondelle, R. *Biophys. J.* **2004**, *86*, 2538.
- Larsen, D. S. *Rev. Sci. Instrum.* **2002**, *72*, 1325.
- Klimov, V. I.; Mikhailovsky, A. A.; McBranch, D. W.; Leatherdale, C. A.; Bawendi, M. G. *Science* **2000**, *287*, 1011.
- van Stokkum, I. H. M.; Larsen, D. S.; van Grondelle, R. *Biochim. Biophys. Acta* **2004**, *1657*, and *1658*, 262 (erratum).
- Csatorday, K.; MacColl, R.; Csizmadia, V.; Grabowski, J.; Bagyinka, C. *Biochemistry* **1984**, *23*, 6466.
- Pearlstein, R. M. In *Photosynthesis*; Amesz, J., Ed.; Elsevier: Amsterdam, 1987; Vol. 15, p 299.
- Scholes, G. D. *Annu. Rev. Phys. Chem.* **2003**, *54*, 57.
- Arnett, D. C.; Moser, C. C.; Dutton, P. L.; Scherer, N. F. *J. Phys. Chem. B* **1999**, *103*, 2014.
- Jonas, D. M.; Lang, M. J.; Nagasawa, Y.; Joo, T.; Fleming, G. R. *J. Phys. Chem.* **1996**, *100*, 12660.
- Polivka, T.; Pullerits, T.; Herek, J. L.; Sundström, V. *J. Phys. Chem. B* **2000**, *104*, 1088.
- Joo, T.; Yiwei, J.; Yu, J.-Y.; Jonas, D. M.; Fleming, G. R. *J. Phys. Chem.* **1996**, *100*, 2399.
- Pullerits, T.; Chachivilis, M.; Jones, M. R.; Hunter, C. N.; Sundström, V. *Chem. Phys. Lett.* **1994**, *224*, 355.
- Hess, S.; Visscher, K. J.; Pullerits, T.; Sundström, V.; Fowler, G. J. S.; Hunter, C. N. *Biochemistry* **1994**, *33*, 8300.
- Novoderezhkin, V.; Monshouwer, R.; van Grondelle, R. *J. Phys. Chem. B* **1999**, *103*, 10540.
- Vos, M. H.; Breton, J.; Martin, J.-L. *J. Phys. Chem. B* **1997**, *101*, 9820.
- Vos, M. H.; Lambry, J.-C.; Robles, S. J.; Youvan, D. C.; Breton, J.; Martin, J.-L. *Proc. Natl. Acad. Sci. U.S.A.* **1992**, *89*, 613.
- Scholes, G. D.; Jordanides, X. J.; Fleming, G. R. *J. Phys. Chem. B* **2001**, *105*, 1640.
- van Grondelle, R.; Dekker, J. P.; Gillbrö, T.; Sundström, V. *Biochim. Biophys. Acta* **1994**, *1187*, 1.
- Novoderezhkin, V.; Wendeling, M.; van Grondelle, R. *J. Phys. Chem. B* **2003**, *107*, 11534.
- Novoderezhkin, V. I.; Palacios, M. A.; van Amerongen, H.; van Grondelle, R. *J. Phys. Chem. B* **2004**, *108*, 10363.
- Stanley, R. J.; King, B.; Boxer, S. G. *J. Phys. Chem.* **1996**, *100*, 12052.